INTERNATIONAL JOURNAL OF CLIMATOLOGY
Int. J. Climatol. **37** (Suppl.1): 1297–1306 (2017)
Published online 30 January 2017 in Wiley Online Library
(wileyonlinelibrary.com) DOI: 10.1002/joc.4993

RMetS
Royal Meteorological Society

Short Communication

Land–atmosphere–aerosol coupling in North China during 2000–2013

Jiangfeng Wei,[a]* Qinjian Jin,[a,b] Zong-Liang Yang[a,c] and Liming Zhou[d]

[a] *Jackson School of Geosciences, University of Texas, Austin, TX, USA*
[b] *Center for Global Change Science, Massachusetts Institute of Technology, Cambridge, MA, USA*
[c] *Key Laboratory of Regional Climate-Environment Research for Temperate East Asia (RCE-TEA), Institute of Atmospheric Physics, Chinese Academy of Sciences, Beijing, China*
[d] *Department of Atmospheric and Environmental Sciences, University at Albany, State University of New York (SUNY), NY, USA*

ABSTRACT: North China is one of the most densely populated regions in the world. To its west, north, and northwest, the world's largest afforestation project has been going on for decades. At the same time, North China has been suffering from air pollution because of its large fossil fuel consumption. Here we show that the changes in land cover and aerosol concentration are coupled with the variations of land surface temperature, cloud cover, and surface solar radiation during the summer 2000–2013. Model experiments show that the interannual variation of aerosol concentration in North China is mainly a result of the varying atmospheric circulation. The increasing vegetation cover due to afforestation has enhanced surface evapotranspiration (ET) and cooled the local surface, and precipitation is observed to be increasing with ET. The model with prescribed increasing vegetation cover can simulate the increasing ET but cannot reproduce the increasing precipitation. Although this may be caused by model biases, the lack of aerosol processes in the model could also be a potential cause.

KEY WORDS land; vegetation; aerosol; China

Received 3 August 2016; Revised 4 November 2016; Accepted 12 December 2016

1. Introduction

Associated with rapid economic development and intense human activities, China has been experiencing dramatic environmental changes. In order to hold back the invasion of Gobi Desert and raise the forest cover in northern China, the Chinese government launched the Three-North Shelterbelt Forest (or the Green Great Wall) Program (Parungo *et al.*, 1994; Tan and Li, 2015). The project was begun in 1978 and is planned to be completed around 2050, when the belt will be 4500 km long. It is by far the world's largest tree-planting project. Studies found that this project has greatly increased the vegetation and decreased the intensity of dust storms in northern China (Parungo *et al.*, 1994; Tan and Li, 2015). On the other hand, the energy consumption in China is rapidly increasing in the past decade and it accounts for two-thirds of the growth in global carbon emission from energy use in this period (Sheehan *et al.*, 2014). In addition to the emission of carbon dioxide, the use of fossil fuel led to serious air pollution that exists as atmospheric aerosols (Luo *et al.*, 2014). North China has one of the highest concentrations of atmospheric aerosols in the world (Remer *et al.*, 2008). These aerosol particles and droplets can directly absorb and scatter solar radiation (Li *et al.*, 2010) and can also indirectly affect radiation and precipitation by changing the macro- and microphysics of clouds (Li *et al.*, 2011; Koren *et al.*, 2012; Niu and Li, 2012). In the past decades, both land use and land cover change and air pollution have attracted great attentions around the world, and their impacts on climate remain unsettled and are still active research topics (e.g. Wu *et al.*, 2013b; Hua *et al.*, 2015; Li *et al.*, 2016; Wu *et al.*, 2016; Zhao *et al.*, 2016). Moreover, the combined influence of the two factors on climate was seldom investigated.

2. Study area

North China is region where both land use and land cover change and air pollution are intense, so it is an ideal place to study their individual and combined effects. The region has strong gradients in topography, vegetation and climate with higher (lower) elevation, sparser (denser) vegetation, and drier (wetter) climate in the northwest (southeast) (Figure S2, Supporting information). Along the southeast-to-northwest line is a semi-arid transitional zone between the wet southeast and dry northwest, where the land surface and climate are sensitive to each other and their interactions are strong (Zhang *et al.*, 2011). This

* Correspondence to: J. Wei, Center for Integrated Earth System Science (CIESS), Jackson School of Geosciences, University of Texas at Austin, 2275 Speedway C9000, Austin, TX 78712, USA. E-mail: jwei@utexas.edu

© 2017 Royal Meteorological Society

transitional zone is also a major region of the Green Great Wall, because its land cover is more fragile and is frequently subjected to the invasion of the desert.

3. Data and methods

3.1. Data

The used datasets include a variety of global climate field from observation-based products or reanalysis. Since the year 2000, various satellite missions provide a large amount of data for the land and atmosphere states and the water and energy fluxes. As the aerosol concentration (Luo *et al.*, 2014) and the vegetation activity and its interaction with climate are all highest during boreal summer in this region, our analyses focus on June–July–August (JJA) 2000–2013. Monthly data were used unless otherwise mentioned.

We used station-based CRU TS3.22 daily maximum near-surface temperature and cloud cover fraction (Harris *et al.*, 2014) at $0.5^\circ \times 0.5^\circ$ resolution.

Several products from the Collection 5 MODerate resolution Imaging Spectroradiometer (MODIS, https://modis.gsfc.nasa.gov/), an instrument onboard the Terra and Aqua satellites, were used, including EVI and NDVI (Huete *et al.*, 2002) (MOD13C2) at $0.05^\circ \times 0.05^\circ$ resolution, Aqua (MYD11C3) and Terra (MOD11C3) LST (Wan, 2008) at $0.05^\circ \times 0.05^\circ$ resolution, and Terra 550 nm AOD (Remer *et al.*, 2005) and Cloud cover fraction (Platnick *et al.*, 2003) (MOD08_M3 v051) at $1^\circ \times 1^\circ$ resolution. Terra LST (10:30 and 22:30 local time) is available from 2000, while Aqua LST (1:30 and 13:30 local time) is available from 2002. As 13:30 local time is close to the time when the surface has the maximum temperature, we used the Aqua LST for this study but extended it to 2000 based on a good linear relationship between Aqua and Terra LST (see Suppporting information).

Two ET data sets were used: MODIS ET product (MOD16A2) at $0.05^\circ \times 0.05^\circ$ resolution from the University of Montana (Mu *et al.*, 2011) and ET from ERA-Interim reanalysis (Dee *et al.*, 2011) at $0.75^\circ \times 0.75^\circ$ resolution. The algorithm for MODIS ET is based on the Penman–Monteith equation driven by MODIS data and daily meteorological data.

In addition to MODIS AOD mentioned above, we also used level 3 MISR (Multi-angle Imaging SpectroRadiometer) (Diner *et al.*, 1998) AOD product (MIL3MAE) at $0.5^\circ \times 0.5^\circ$ resolution. MISR is a key instrument aboard the Terra satellite in a sun-synchronous orbit. MISR acquires systematic multi-angle imagery for global monitoring of top-of-atmosphere and surface albedos and to measure the shortwave radiative properties of aerosols, clouds and surface scenes in order to characterize their impact on the Earth's climate.

We used the monthly surface downward solar radiation data from the Clouds and the Earth's Radiant Energy System (CERES) (Wielicki *et al.*, 1996) Edition 2.8 at $1^\circ \times 1^\circ$ resolution. CERES instruments are collecting observations on three separate satellite missions, including Terra and Aqua observatories and the Suomi National Polar-orbiting Partnership (S-NPP) observatory. CERES products include both solar-reflected and Earth-emitted radiation from the top-of-atmosphere to the Earth's surface.

For precipitation data, we used Tropical Rainfall Measuring Mission (TRMM) (Huffman *et al.*, 2007) 3B43 precipitation data at $0.25^\circ \times 0.25^\circ$ resolution and PRECipitation REConstruction over Land (PREC/L) precipitation data (Chen *et al.*, 2002) at $1^\circ \times 1^\circ$ resolution. TRMM 3B43 provides the best-estimate precipitation rate and root-mean-square precipitation-error estimate field by combining the 3-hourly merged-infrared estimates with the monthly-accumulated Global Precipitation Climatology Centre (GPCC) rain gauge analysis. PREC/L was produced by interpolation of gauge observations over land.

3.2. MV-EOF analysis

Multivariate empirical orthogonal function (MV-EOF) analysis is the same as the traditional EOF analysis or principal component analysis except that two or more variables are used. As the variables may have different units and variances, each variable is standardized by its mean standardized deviation in the spatial domain. Thus, the variances of different variables are comparable and each variable maintains its own spatial distribution of variance. As the time dimensions of the variables are the same, they are combined into a new variable along a spatial dimension (longitude or latitude). Then a tradition EOF analysis is performed for the combined new variable. The results are the strongest principal component time series and the associated spatial patterns for the combined variable, which can be decomposed in the way the original variables are combined to get the spatial patterns of the original variables.

3.3. WRF simulations

We designed regional climate model simulations with the Weather Research and Forecast (WRF) model (Skamarock *et al.*, 2008) (version 3.5) to investigate the effects of vegetation change and aerosols. The model resolution was 36 km and has 30 vertical levels. The initial and boundary conditions (including SST) were from ERA-Interim reanalysis (Dee *et al.*, 2011) 6-hourly data. The spatial domain of the simulations is shown in Figure S5. Two experiments were performed for 2000–2013. In the control experiment (WRF_CTL), the vegetation state was kept the same as the year 2000 (with a seasonal cycle) and did not change from year to year. In the other experiment (WRF_VEG), the monthly vegetation in the model was prescribed according to MODIS-based datasets of leaf area index (LAI) (Yuan *et al.*, 2011) and albedo (Liu *et al.*, 2013). We performed simulations for 1 May to 31 August of each year in 2000 to 2013, and the data in JJA were used for analysis. Vegetation fraction was updated according to the LAI. Each experiment has 14 ensemble members with different combinations of physical parameterizations (see Supporting Information).

The model has a globally constant near-zero aerosol field, and the influence of aerosols on clouds is not

© 2017 Royal Meteorological Society

considered (due to the large uncertainties and high computational cost of the aerosol-related module, we did not use it for this study). Nevertheless, the role of aerosols can be inferred by comparing model results with observations. If the model can simulate an observed variability, then the aerosols should not be an important factor for this variability. While if the model cannot simulate an observed variability, there is a possibility that aerosols play a role in this variability, although the model deficiency is also a possible factor.

4. Results

4.1. Observational analysis

We first look at the land surface changes using satellite-derived Enhanced Vegetation Index (EVI), Normalized Difference Vegetation Index (NDVI), evapotranspiration (ET) and land surface temperature (LST). The vegetation activity (EVI and NDVI) and ET show significant increasing trends in the transitional zone, where LST shows a significant cooling trend (Figure 1). These are evident signals of the Green Great Wall. A multivariate Empirical Orthogonal Function (MV-EOF) analysis (see Methods) is used to find the consistent large-scale interannual variability of EVI and ET and reduce the noise and uncertainties from a single dataset and at a few grid points. ET is selected because it is closely related to the surface water and energy balance and it would be interesting to find out its relationship with vegetation. Figure 2 (top) shows the dominant mode from the MV-EOF analysis of EVI and ET, which explains 41.9% of the total variance. The dominant mode shows an evident increasing trend of EVI and ET in the transitional zone, consistent with the spatial patterns of their trends in Figure 1. The similarity of the patterns of EVI and ET changes indicates a strong local coupling between them.

To reduce the uncertainties in satellite observations of aerosol concentration, we performed an MV-EOF analysis for the AOD (aerosol optical depth) datasets from two different sensors: MODIS and MISR, both onboard the Terra satellite. Their dominant mode, occupying 48% of the total variance, shows a similar pattern for the two datasets, with the strongest variability in the central North China Plain (Figure 2 bottom). This region also has the highest average AOD (Luo *et al.*, 2014). The first principal component (PC1) time series shows a strong interannual variability but no evident trend. This time series is very similar to the variations of the average AOD in the domain (not shown). Although the total use of fossil fuels in the region was increasing, the use of cleaner energy sources and the introduction of more efficient equipment have reduced the emissions (Chan and Yao, 2008; Sheehan *et al.*, 2014). This may be the reason for the absence of AOD trend; we will discuss its interannual variations later.

Afforestation usually leads to more transpiration and higher ET, which can cool the surface. Aerosols from anthropogenic emissions can block the downward solar radiation and cool the surface too. In addition to these direct effects on surface temperature, both of them can affect clouds. Increased ET provides more moisture for cloud formation. The influence of aerosols on clouds are complicated, but most observations show that in a wet region like the North China Plain and during the monsoon season aerosols can enhance the development of clouds and increase the frequency and intensity of precipitation (Li *et al.*, 2011; Koren *et al.*, 2012). Thus, both afforestation and aerosols can cool the surface directly and indirectly. Local correlations between the vegetation index (EVI) or aerosol index (AOD) and surface temperature show predominantly negative correlations (Figure S3), especially over the regions where vegetation or aerosols have large variabilities (Figure 2). This confirms the possible cooling effects of vegetation and aerosols, but the exactly influence pathways, especially whether clouds are involved, are unclear.

To investigate the coupling of surface temperature, cloud cover, and surface solar radiation, we performed an MV-EOF analysis for the three variables. Surface daily maximum temperature (T_{max}) and cloud cover fraction are from a station-based Climate Research Unit (CRU) dataset, and surface downward solar radiation (R_s) is from a satellite-based Clouds and the Earth's Radiant Energy System (CERES) dataset. Figure 3 shows the two dominant modes. In both modes, the three variables show similar spatial patterns (cloud fraction varies oppositely to the other two), indicating that they are strongly locally coupled. PC1 time series is significantly correlated with the AOD variations in the area ($P < 0.01$), and spatially the largest variability is in the central North China Plain, where AOD has the largest variability (Figure 2). This result alone does not tell us why AOD is related to the variations of T_{max}, clouds, and R_s. It is possible that aerosols affect the clouds, or they are both controlled by the variations of some other factors such as atmospheric circulation. This needs further investigation. PC2 time series shows a trend and is significantly correlated with the EVI and ET variations ($P < 0.02$). The associated surface cooling, increasing cloud, and decreasing R_s are strongest in the northern North China Plain. Again, the result does not tell a causal relationship. The vegetation and ET increases could increase moisture (Jiang and Liang, 2013) and cloud cover in the northern plain and decrease surface temperature. It is also possible that the vegetation and ET respond to the increasing cloud and precipitation (Figures 6(a) and (b)). Although human afforestation should be the main reason for the vegetation increase in this area, the positive vegetation-precipitation feedback (Zhang *et al.*, 2003; Liu *et al.*, 2006) could also play a role, especially in such a semi-arid region. Global warming can also enhance the vegetation activity (Zhou *et al.*, 2001), but considering the recent warming hiatus (Li *et al.*, 2015) and the length of our study period, it should not have a major influence.

Similar results as in Figure 3 can be obtained if replacing the CRU T_{max} and cloud cover fraction with MODIS LST (13:30) and cloud cover (Figure S4). Although MODIS LST is retrieved under clear-sky conditions, the influence of clouds and especially precipitation during cloudy days

© 2017 Royal Meteorological Society

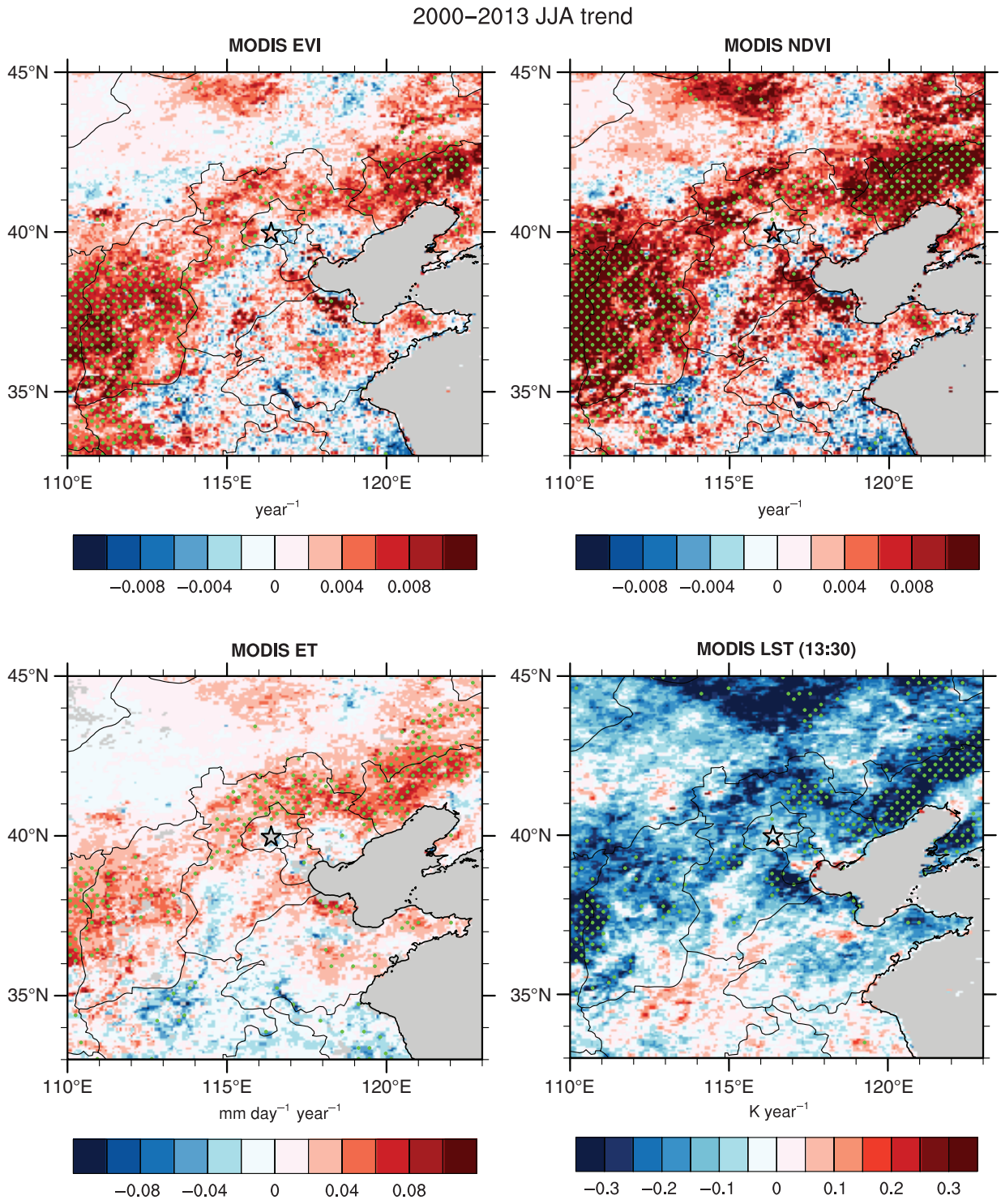

Figure 1. The linear trend of JJA 2000–2013 EVI, NDVI, ET and LST at 13:30. Data derived from MODIS satellite data. The green stippling highlights the trends that are 90% confident. The stars show the location of Beijing city. Note that MODIS LST is the near-surface temperature retrieved under clear-sky conditions, so it is less affected by cloud variations and shows stronger relationships with surface changes than the all-sky 2 m air temperature from stations (e.g. CRU data).

can be memorized by the land surface and brought to clear-sky days.

4.2. Model simulations

Figure 4(a) shows that the model, without aerosol processes, can simulate the observed interannual variability of T_{max} and R_s in North China quite well. This suggests that aerosols do not have a major influence on their variability. The simulated precipitation and ET are not so consistent with observations, a common feature of most weather and climate models. With changing vegetation cover, experiment WRF_VEG simulates lower T_{max} and higher ET

© 2017 Royal Meteorological Society

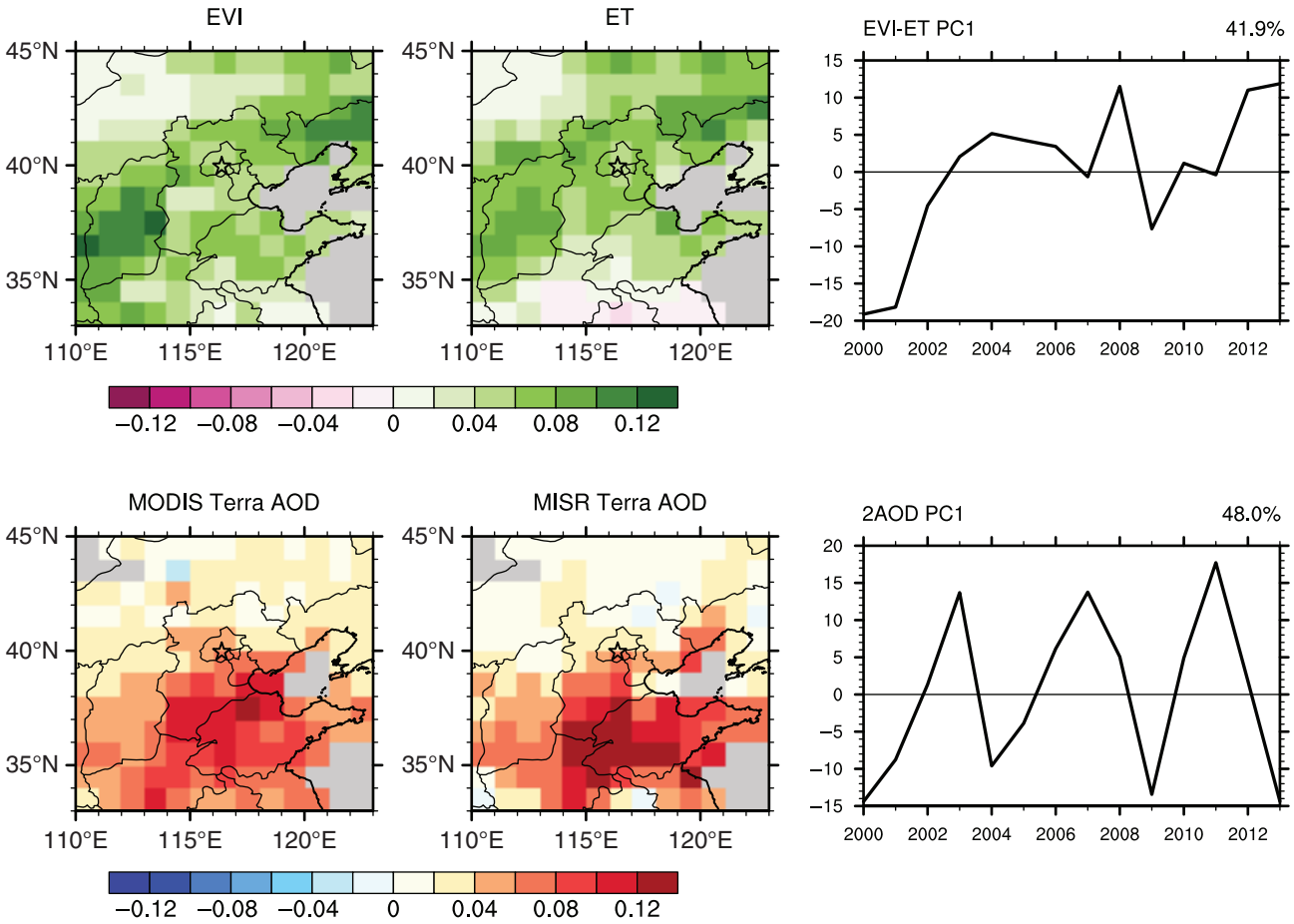

Figure 2. MV-EOF analyses showing the dominant interannual variations of land cover and aerosols during JJA 2000–2013. Top panels are for MODIS EVI and ET and bottom panels are for AOD from MODIS Terra and MISR Terra. Both the dominant EOF patterns and the associated PC time series are shown. The percentage variance explained by each dominant mode is shown at the top right corner of the time series.

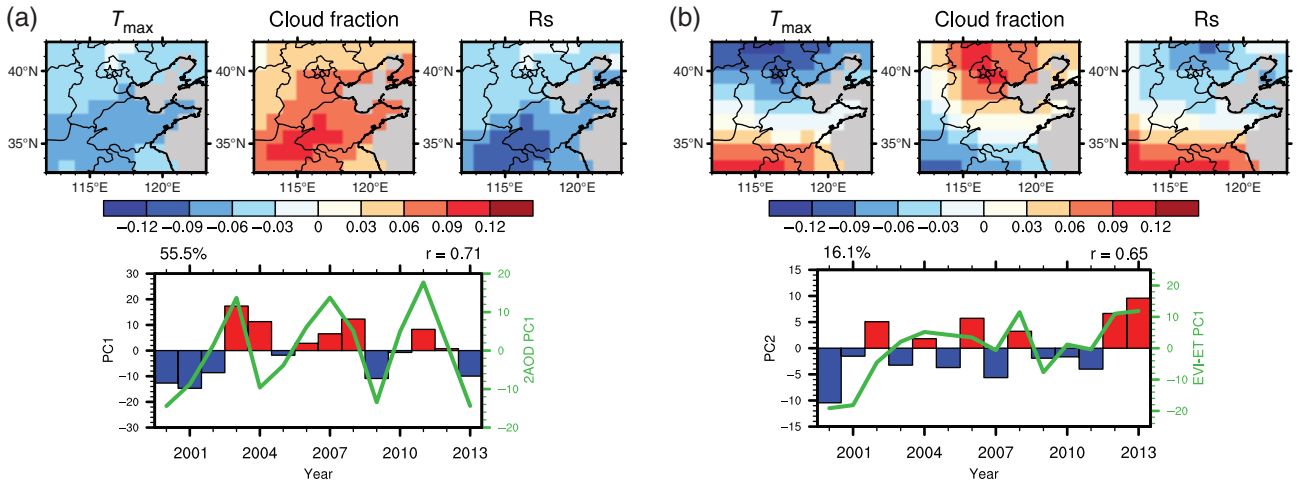

Figure 3. MV-EOF analysis showing the interannual coupling of T_{max} (CRU), cloud cover fraction (CRU) and surface incident solar radiation (CERES) during JJA 2000–2013. (a) First mode. (b) Second mode. Top panels show the EOF patterns (unitless), and the bars in bottom panels show the associated principal component (PC) time series. The green lines are (a) the PC1 time series of the two AOD products (Figure 2) and (b) the PC1 time series of EVI and ET (Figure 2). The percentage variance explained by each mode are shown at the top left of the bottom panels, and the correlations between the bars and green lines are shown at the top right of the bottom panels. Note that the MV-EOF in this figure is performed in a smaller spatial domain than in Figure 2 in order to capture the EOF modes associated with both aerosols and vegetation.

© 2017 Royal Meteorological Society

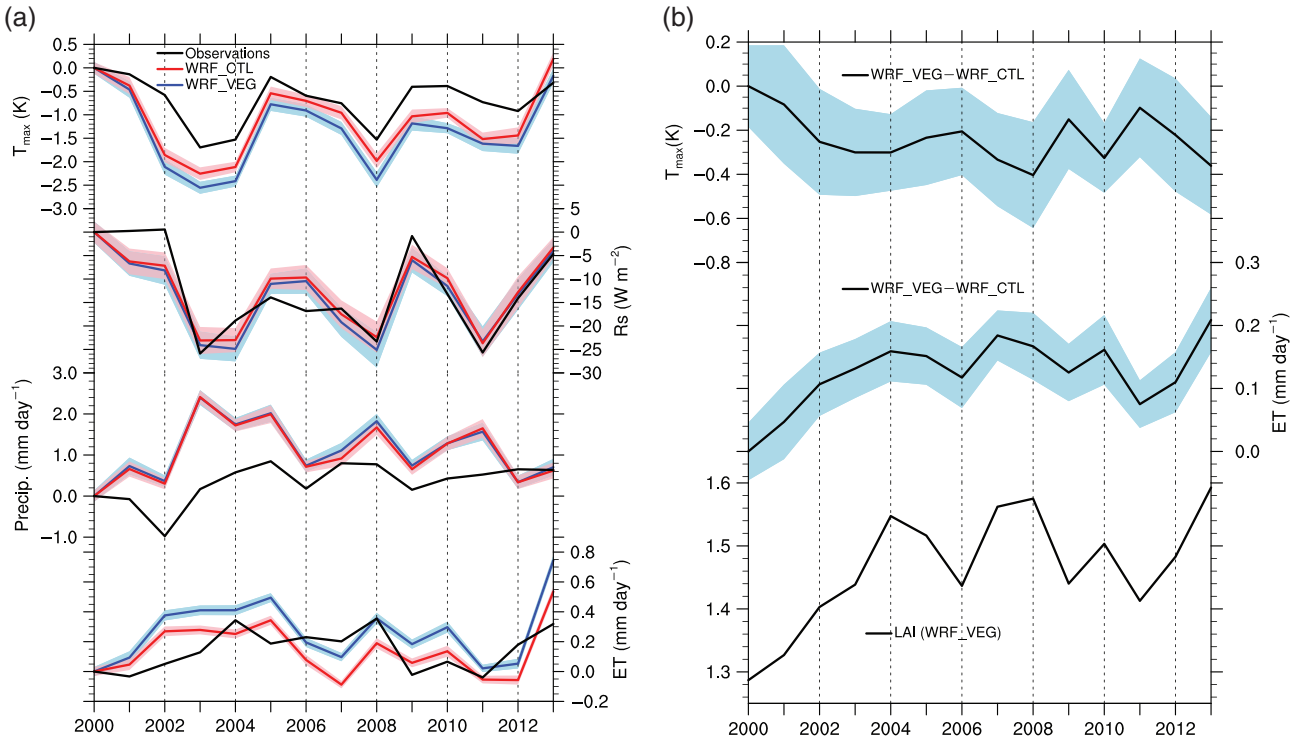

Figure 4. Results from WRF experiments. (a) JJA 2000–2013 interannual anomaly (from 2000) of average T_{max}, R_S, precipitation, and ET over North China (33°–42°N, 112°–123°E; area in Figure 3) from two model experiments and observations. (b) The difference in T_{max} and ET between the two experiments (WRF_VEG – WRF_CTL) and the average LAI prescribed in the WRF_VEG experiment. The shadings show the stand errors of the 14 ensemble members. The observational data for T_{max}, R_s, precipitation and ET are from CRU, CERES, PREC/L and MODIS, respectively.

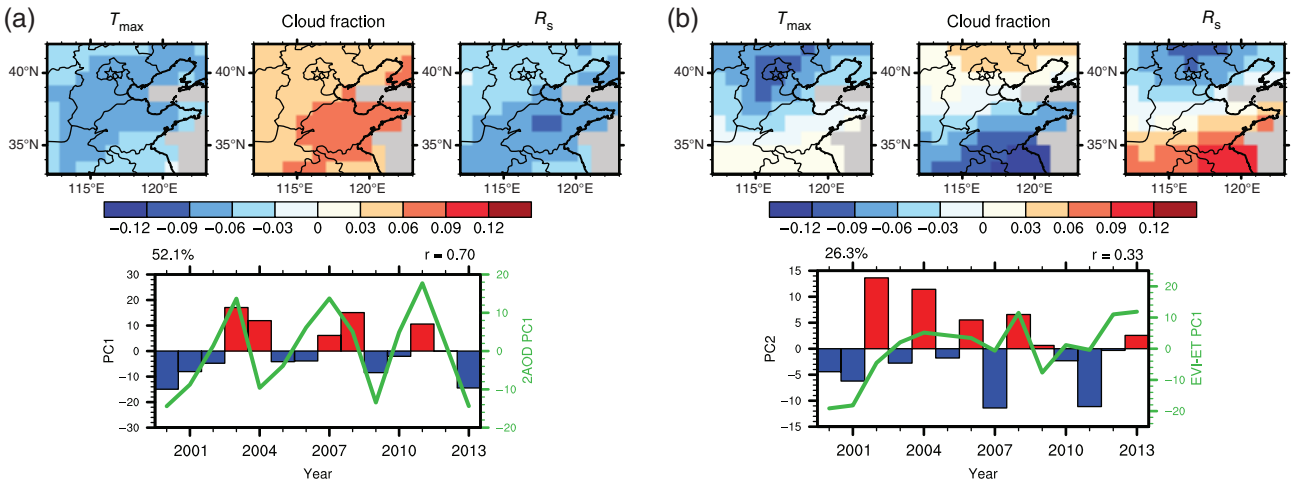

Figure 5. Same as Figure 3 but for the variables from WRF_VEG experiment. WRF_CTL shows very similar results (not shown). The two green lines are the same as in Figure 3.

than the control experiment WRF_CTL. Their differences (WRF_VEG – WRF_CTL) are highly consistent with the variation of LAI (Figure 4(b)). The spatial patterns of the differences in surface temperature and ET are also very similar to the pattern of LAI change (Figure S5). It is evident that the enhanced vegetation activity increases ET and cools the surface. The differences in R_s and precipitation between WRF_CTL and WRF_VEG are less significant, but R_s decreases slightly and precipitation increases slightly in WRF_VEG compared to WRF_CTL, an indication of slightly increased cloudiness.

To further compare the model results with observations, we performed the same MV-EOF analysis as in Figure 3 but using the model output (Figure 5). The two experiments show similar results, which capture the dominant coupled variability of T_{max}, cloud cover, and R_s, but the second variability mode associated with vegetation and ET variations is not captured. The model does not consider the influence of varying aerosol concentrations, but the variability of the first mode, same as in observations, is still very similar to that of AOD. This result, along with those in Figure 4(a), indicate that this dominant variability is not

© 2017 Royal Meteorological Society

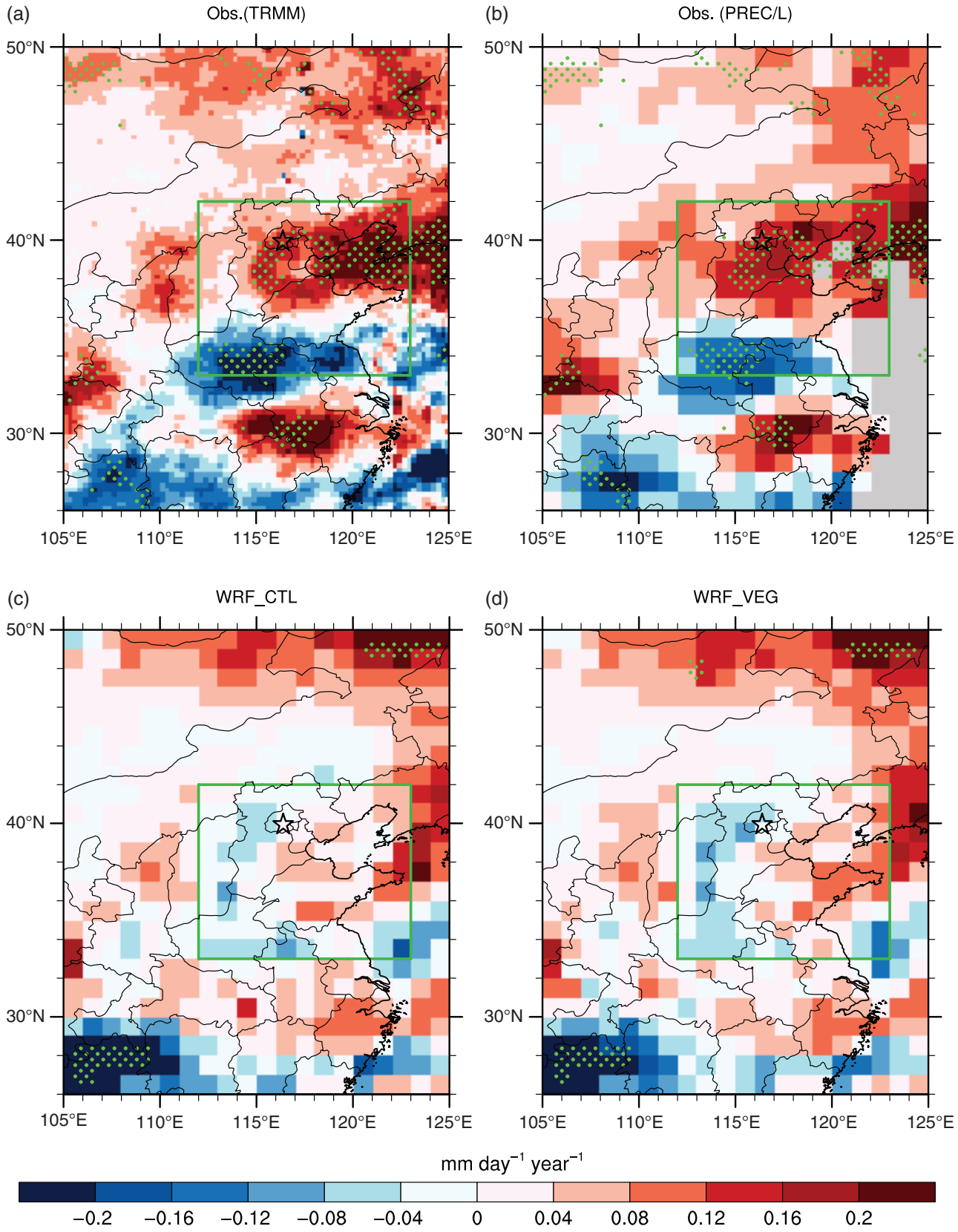

Figure 6. Precipitation linear trend during JJA 2000–2013. (a) TRMM. (b) PREC/L. (c) Average of WRF_CTL ensembles. (d) Average of WRF_VEG ensembles. The green stippling highlights the trends that are 90% confident. The green box encloses the region for MV-EOF analyses (Figures 3 and 5).

© 2017 Royal Meteorological Society

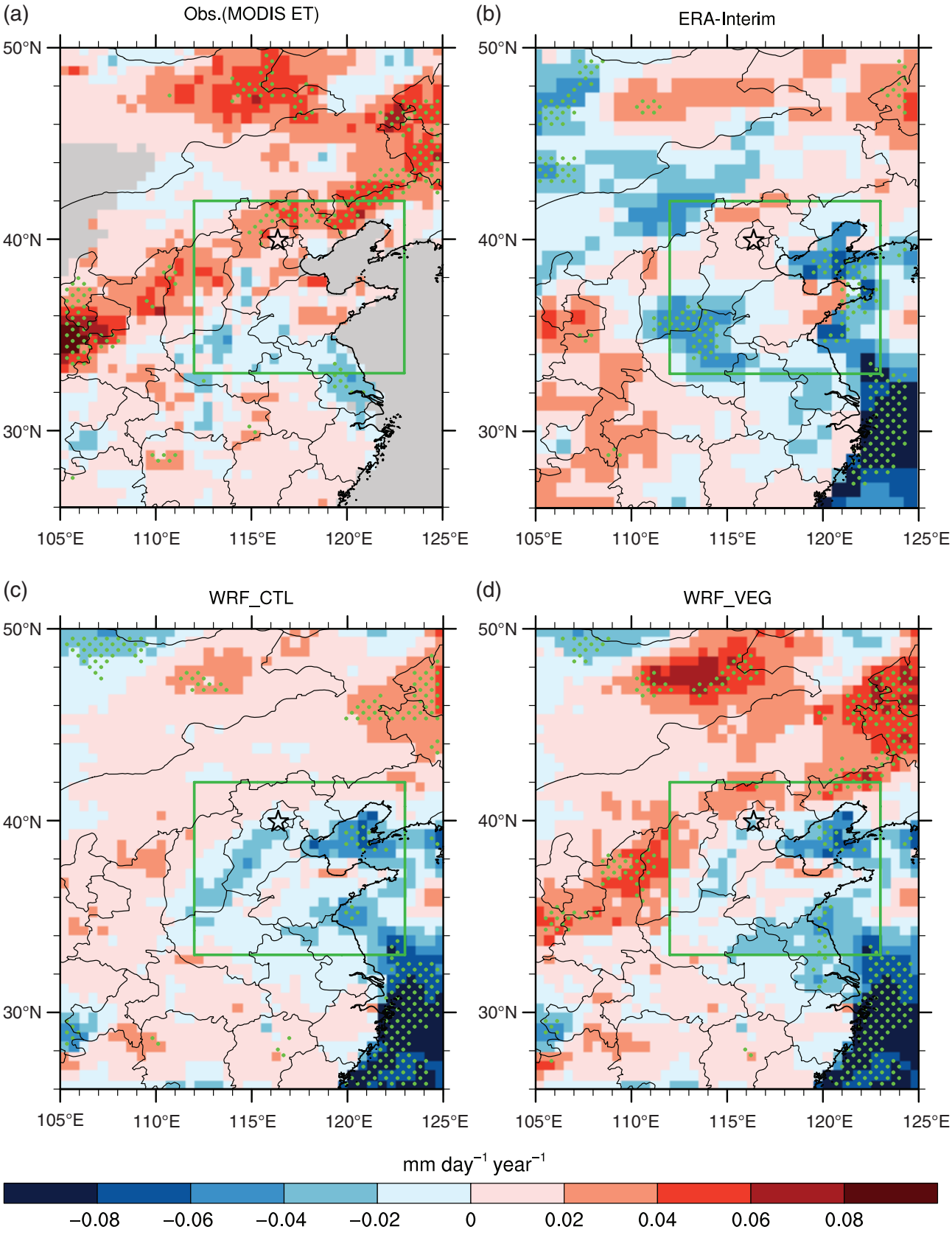

Figure 7. Same as Figure 6 but for ET. (a) MODIS ET. (b) ERA-Interim ET. (c) Average of WRF_CTL ensembles. (d) Average of WRF_VEG ensembles.

© 2017 Royal Meteorological Society

caused by aerosols, and the interannual variations of atmospheric circulation may have controlled both this variability and the variations of AOD in North China. It is found that the cloud cover and AOD in North China are strongly associated with the monsoon circulation (Figure S6). As found in a previous study (Yan *et al.*, 2011), a stronger East Asian summer monsoon can lead to higher AOD and more cloud and precipitation in North China, and the effect of wet deposition is secondary.

For the second mode (Figure 5(b) *vs* Figure 3(b)), the coupled patterns of the three variables and their interannual variations are properly simulated, and the bias is mainly in the decadal variation or trend, which is usually related to some external forcing. This bias can be clearly seen in the trends of precipitation (Figure 6) as wells as the cloud cover (not shown) but the former has more accurate and consistent observations. The observed dipole pattern of precipitation trends in North China (increasing in the north and decreasing in the south), which is similar to that in the second mode of the MV-EOF analysis (Figure 3(b)), is not simulated by both experiments. We also checked each of the 14 ensemble members. Although some of them show areas of stronger increasing trends of precipitation in WRF_VEG than in WRF_CTL, none of them show the observed dipole pattern of significant precipitation trends. What is the source of this model bias?

Figure 7 shows the ET trends from a MODIS-based product, ERA-Interim, and the two model experiments. MODIS ET shows significant increasing trends in the transitional zone, which are not seen in ERA-Interim or the experiment WRF_CTL, but the experiment WRF_VEG produces the trends quite well. ERA-Interim was constrained by observations, but it did not consider the changing vegetation cover, and its precipitation and ET were produced by the assimilation model (not observed). WRF_CTL also did not consider the changing vegetation. These explain why ERA-Interim and CTL cannot produce the observed ET trends. Although WRF_VEG produced the observed increasing ET in the transitional zone, it did not produce the increasing trend of precipitation (Figure 6). This indicates that the model may not correctly simulate the response of precipitation to ET, a key process in land–atmosphere interactions. It is also possible that the increasing trend of precipitation is not a result of the increasing ET, and due to some model biases, both experiments do not capture this trend. It is difficult to pinpoint the exactly physical processes where the model has biases. It could be in the parameterizations of the boundary layer, the cumulus convection, or the microphysics. Nevertheless, the differences in simulated precipitation trends are mainly in North China, where the aerosol concentration is the highest (Figure 6). This suggests that the lack of aerosols processes in the model could be an important reason for these differences. Although the aerosol concentration in North China does not show a trend (Figure 2), aerosols may influence the response of clouds and precipitation to surface ET, and the influence of aerosol indirect effects on convection and precipitation can be positive or negative, depending on the atmosphere and cloud conditions (Koren *et al.*, 2008; Fan *et al.*, 2009; Li *et al.*, 2011; Niu and Li, 2012) and aerosol composition (Fan *et al.*, 2008). In addition, aerosol direct effect can lead to heating in the atmosphere and cooling at surface, which may affect the regional atmospheric circulation (Wu *et al.*, 2013a). Due to the complex nature of the influence of aerosols on precipitation and the high computational cost of aerosol simulations, the exact influence of aerosols on the trends of clouds and precipitation in North China will be left for future study.

5. Concluding remarks

Land use and land cover change and air pollution are two major environmental concerns of human society, and they also influence long-term climate change. In some regions, like North China, rapid urbanization and industrialization have caused dramatically environmental changes. At the same time, large-scale man-made afforestation was implemented in this region to mitigate environmental consequences. Most previous studies have focused on individual research topics, but few studies have considered them together. Here we find that afforestation not only reduces global warming in North China by enhancing surface ET and but also probably interacts with aerosols to modify regional hydrological and radiative processes. Aerosols may influence land–atmosphere interactions and change the results of long-term climate projections. Current climate models have begun to include detailed representations of aerosols and their direct and indirect effects (Grell *et al.*, 2005), but large uncertainties remain and more work needs to be done (Ghan and Schwartz, 2007). The complex land–atmosphere–aerosol interactions should be paid more attention in future climate projections, especially in regions with high aerosol concentrations.

Acknowledgements

This study was supported by the National Key Research and Development Program of China (Grant No. 2016YFA0600403) and funds from the Jackson School of Geosciences at the University of Texas at Austin.

Supporting information

The following supporting information is available as part of the online article:

Appendix S1. Supporting information.

References

Chan CK, Yao X. 2008. Air pollution in mega cities in China. *Atmos. Environ.* **42**: 1–42.

Chen MY, Xie PP, Janowiak JE, Arkin PA. 2002. Global land precipitation: a 50-yr monthly analysis based on gauge observations. *J. Hydrometeorol.* **3**: 249–266.

© 2017 Royal Meteorological Society

Dee DP, Uppala SM, Simmons AJ, Berrisford P, Poli P, Kobayashi S, Andrae U, Balmaseda MA, Balsamo G, Bauer P, Bechtold P, Beljaars ACM, van de Berg L, Bidlot J, Bormann N, Delsol C, Dragani R, Fuentes M, Geer AJ, Haimberger L, Healy SB, Hersbach H, Hólm EV, Isaksen L, Kållberg P, Köhler M, Matricardi M, McNally AP, Monge-Sanz BM, Morcrette JJ, Park BK, Peubey C, de Rosnay P, Tavolato C, Thépaut JN, Vitart F. 2011. The ERA-Interim reanalysis: configuration and performance of the data assimilation system. *Q. J. Roy. Meteorol. Soc.* **137**: 553–597.

Diner DJ, Beckert JC, Reilly TH, Bruegge CJ, Conel JE, Kahn RA, Martonchik JV, Ackerman TP, Davies R, Gerstl SAW, Gordon HR, Muller JP, Myneni RB, Sellers PJ, Pinty B, Verstraete MM. 1998. Multi-angle Imaging SpectroRadiometer (MISR) instrument description and experiment overview. *IEEE Trans. Geosci. Remote Sens.* **36**: 1072–1087.

Fan JW, Zhang RY, Tao WK, Mohr KI. 2008. Effects of aerosol optical properties on deep convective clouds and radiative forcing. *J. Geophys. Res.* **113**: D08209, doi: 10.1029/2007jd009257.

Fan JW, Yuan TL, Comstock JM, Ghan S, Khain A, Leung LR, Li ZQ, Martins VJ, Ovchinnikov M. 2009. Dominant role by vertical wind shear in regulating aerosol effects on deep convective clouds. *J. Geophys. Res.* **114**: D22206, doi: 10.1029/2009JD012352.

Ghan SJ, Schwartz SE. 2007. Aerosol properties and processes: a path from field and laboratory measurements to global climate models. *Bull. Am. Meteorol. Soc.* **88**: 1059–1083.

Grell GA, Peckham SE, Schmitz R, McKeen SA, Frost G, Skamarock WC, Eder B. 2005. Fully coupled "online" chemistry within the WRF model. *Atmos. Environ.* **39**: 6957–6975.

Harris I, Jones PD, Osborn TJ, Lister DH. 2014. Updated high-resolution grids of monthly climatic observations – the CRU TS3.10 Dataset. *Int. J. Climatol.* **34**: 623–642.

Hua WJ, Chen HS, Li X. 2015. Effects of future land use change on the regional climate in China. *Sci. China-Earth Sci.* **58**: 1840–1848.

Huete A, Didan K, Miura T, Rodriguez EP, Gao X, Ferreira LG. 2002. Overview of the radiometric and biophysical performance of the MODIS vegetation indices. *Remote Sens. Environ.* **83**: 195–213.

Huffman GJ, Adler RF, Bolvin DT, Gu GJ, Nelkin EJ, Bowman KP, Hong Y, Stocker EF, Wolff DB. 2007. The TRMM multisatellite precipitation analysis (TMPA): quasi-global, multiyear, combined-sensor precipitation estimates at fine scales. *J. Hydrometeorol.* **8**: 38–55.

Jiang B, Liang S. 2013. Improved vegetation greenness increases summer atmospheric water vapor over Northern China. *J. Geophys. Res.* **118**: 8129–8139.

Koren I, Martins JV, Remer LA, Afargan H. 2008. Smoke invigoration versus inhibition of clouds over the Amazon. *Science* **321**: 946–949.

Koren I, Altaratz O, Remer LA, Feingold G, Martins JV, Heiblum RH. 2012. Aerosol-induced intensification of rain from the tropics to the mid-latitudes. *Nat. Geosci.* **5**: 118–122.

Li ZQ, Lee KH, Wang YS, Xin JY, Hao WM. 2010. First observation-based estimates of cloud-free aerosol radiative forcing across China. *J. Geophys. Res.* **115**, doi: 10.1029/2009jd013306.

Li Z, Niu F, Fan J, Liu Y, Rosenfeld D, Ding Y. 2011. Long-term impacts of aerosols on the vertical development of clouds and precipitation. *Nat. Geosci.* **4**: 888–894.

Li Q, Yang S, Xu W, Wang XL, Jones P, Parker D, Zhou L, Feng Y, Gao Y. 2015. China experiencing the recent warming hiatus. *Geophys. Res. Lett.* **42**: 889–898.

Li CX, Zhao TB, Ying KR. 2016. Effects of anthropogenic aerosols on temperature changes in China during the twentieth century based on CMIP5 models. *Theor. Appl. Climatol.* **125**: 529–540.

Liu Z, Notaro M, Kutzbach J, Liu N. 2006. Assessing global vegetation–climate feedbacks from observations. *J. Clim.* **19**: 787–814.

Liu Q, Wang L, Qu Y, Liu N, Liu S, Tang H, Liang S. 2013. Preliminary evaluation of the long-term GLASS albedo product. *Int. J. Digital Earth* **6**: 69–95.

Luo Y, Zheng X, Zhao T, Chen J. 2014. A climatology of aerosol optical depth over China from recent 10 years of MODIS remote sensing data. *Int. J. Climatol.* **34**: 863–870.

Mu QZ, Zhao MS, Running SW. 2011. Improvements to a MODIS global terrestrial evapotranspiration algorithm. *Remote Sens. Environ.* **115**: 1781–1800.

Niu F, Li ZQ. 2012. Systematic variations of cloud top temperature and precipitation rate with aerosols over the global tropics. *Atmos. Chem. Phys.* **12**: 8491–8498.

Parungo F, Li Z, Li X, Yang D, Harris J. 1994. Gobi dust storms and The Great Green Wall. *Geophys. Res. Lett.* **21**: 999–1002.

Platnick S, King MD, Ackerman SA, Menzel WP, Baum BA, Riedi JC, Frey RA. 2003. The MODIS cloud products: algorithms and examples from Terra. *IEEE Trans. Geosci. Remote Sens.* **41**: 459–473.

Remer LA, Kaufman YJ, Tanré D, Mattoo S, Chu DA, Martins JV, Li RR, Ichoku C, Levy RC, Kleidman RG, Eck TF, Vermote E, Holben BN. 2005. The MODIS aerosol algorithm, products, and validation. *J. Atmos. Sci.* **62**: 947–973.

Remer LA, Kleidman RG, Levy RC, Kaufman YJ, Tanre D, Mattoo S, Martins JV, Ichoku C, Koren I, Yu HB, Holben BN. 2008. Global aerosol climatology from the MODIS satellite sensors. *J. Geophys. Res.* **113**: D14S07, doi: 10.1029/2007JD009661.

Sheehan P, Cheng EJ, English A, Sun FH. 2014. China's response to the air pollution shock. *Nat. Clim. Change* **4**: 306–309.

Skamarock, W, Klemp JB, Dudhia J, Gill DO, Barker D, Duda MG, Huang X-Y, Wang W. 2008: A description of the advanced research WRF version 3. NCAR Technical Note, doi: 10.5065/D68S4MVH

Tan M, Li X. 2015. Does the Green Great Wall effectively decrease dust storm intensity in China? A study based on NOAA NDVI and weather station data. *Land Use Policy* **43**: 42–47.

Wan Z. 2008. New refinements and validation of the MODIS land-surface temperature/emissivity products. *Remote Sens. Environ.* **112**: 59–74.

Wielicki BA, Barkstrom BR, Harrison EF, Lee RB, Louis Smith G, Cooper JE. 1996. Clouds and the Earth's Radiant Energy System (CERES): an earth observing system experiment. *Bull. Am. Meteorol. Soc.* **77**: 853–868.

Wu LT, Su H, Jiang JH. 2013a. Regional simulation of aerosol impacts on precipitation during the East Asian summer monsoon. *J. Geophys. Res.* **118**: 6454–6467.

Wu PL, Christidis N, Stott P. 2013b. Anthropogenic impact on Earth's hydrological cycle. *Nat. Clim. Change* **3**: 807–810.

Wu GX, Li ZQ, Fu CB, Zhang XY, Zhang RY, Zhang RH, Zhou TJ, Li JP, Li JD, Zhou DG, Wu L, Zhou LT, He B, Huang RH. 2016. Advances in studying interactions between aerosols and monsoon in China. *Sci. China-Earth Sci.* **59**: 1–16.

Yan L, Liu X, Yang P, Yin Z-Y, North GR. 2011. Study of the impact of summer monsoon circulation on spatial distribution of aerosols in East Asia based on numerical simulations. *J. Appl. Meteorol. Climatol.* **50**: 2270–2282.

Yuan H, Dai YJ, Xiao ZQ, Ji DY, Shangguan W. 2011. Reprocessing the MODIS Leaf Area Index products for land surface and climate modelling. *Remote Sens. Environ.* **115**: 1171–1187.

Zhang J, Dong W, Ye D, Fu C. 2003. New evidence for effects of land cover in China on summer climate. *Chin. Sci. Bull.* **48**: 401–405.

Zhang JY, Wu LY, Dong WJ. 2011. Land-atmosphere coupling and summer climate variability over East Asia. *J. Geophys. Res.* **116**: D05117, doi: 10.1029/2010JD014714.

Zhao TB, Li CX, Zuo ZY. 2016. Contributions of anthropogenic and external natural forcings to climate changes over China based on CMIP5 model simulations. *Science China-Earth Sciences* **59**: 503–517.

Zhou L, Tucker CJ, Kaufmann RK, Slayback D, Shabanov NV, Myneni RB. 2001. Variations in northern vegetation activity inferred from satellite data of vegetation index during 1981 to 1999. *J. Geophys. Res.* **106**: 20069–20083.

© 2017 Royal Meteorological Society